This is a repository copy of *Making the right link to theranostics : the photophysical and biological properties of dinuclear Ru^II-Re^I dppz complexes depend on their tether*.

Version: Accepted Version

Article:

Making the right link to theranostics: the photophysical and biological properties of dinuclear Ru^{II}-Re^{I} dppz complexes depend on their tether.

Hiwa K. Saeed,[†▲] Sreejesh Sreedharan, [†◆] Paul J. Jarman,[‡] Stuart A. Archer,[†] Simon D Fairbanks,[†] Simon P Foxon,[§] Alexander J. Auty, [†] Dimitri Chekulaev, [†] Theo Keane, [†] Anthony J. H. M. Meijer, [†] Julia A. Weinstein, [†] Carl G. W. Smythe,[‡] Jorge Bernardino de la Serna,[II⊥] and Jim A. Thomas*[†].

[†]Department of Chemistry, and [‡]Department of Biomedical Science, University of Sheffield, Sheffield S10 2TN, United Kingdom.

[§]ZapGo Ltd, Rutherford Appleton Laboratory, Harwell, Oxford OX11 0FA, United Kingdom.

[II]Central Laser Facility, Rutherford Appleton Laboratory, Research Complex at Harwell, Science and Technology Facilities Council, Harwell-Oxford, Didcot OX11 0QX, United Kingdom

⊥ National Heart and Lung Institute, Faculty of Medicine, Imperial College London, Sir Alexander Fleming Building, Exhibition Road, London, SW7 2AZ, United Kingdom

ABSTRACT: The synthesis of a new dinuclear complexes containing linked Ru^{II}(dppz) and Re^{I}(dppz) moieties is reported. The photophysical and biological properties of the new complex, which incorporates a *N,N'*-bis(4-pyridylmethyl)-1,6-hexanediamine tether ligand, are compared to a previously reported Ru^{II}/Re^{I} complex linked by a simple dipyridyl alkane ligand. Although both complexes bind to DNA with similar affinities, steady state and time resolved photophysical studies reveal that the nature of the linker affects the excited state dynamics of the complexes and their DNA photocleavage properties. Quantum based DFT calculations on these systems offers insights into these effects. Whilst both complexes are live cells permeant, their intracellular localization are significantly affected by the nature of the linker. Notably, one of the complexes displayed concentration dependent localization and possesses photophysical properties that are compatible with SIM and STED nanoscopy. This allowed the dynamics of its intracellular localization to be tracked at super resolutions.

Introduction

Luminescent d^6-metal complexes that interact with biomolecules, such as DNA, offer excellent potential as imaging probes and as tools to investigate processes such as electron transfer within a biological context.[1-8] The "DNA light switch" $[Ru(LL)_2(dppz)]^{2+}$ (dppz = dipyrido[3,2-a:2',3'-c]phenazine, LL = bidentate ligands such as 2,2'-bipyridine and 1,10-phenanthroline) is a well-known example of a complex studied towards these goals. It has attracted particular attention as it displays a huge luminescence enhancement ($>10^4$) upon intercalation into DNA.[9]

Although the chloride salt of the parent complex is not taken up by live cells, derivatives that function as cell probes for DNA have been reported[10,11] Given that these complexes target DNA their potential as therapeutics and phototherapeutics has also been explored. [12-14] While the excited state of $[Ru(LL)_2(dppz)]^{2+}$ itself is not sufficiently oxidizing to cleave DNA directly and the intercalated species is a poor singlet oxygen sensitizer,[15] complexes with related ancillary ligands[16,17] or suitably substituted dppz ligands show promising photo-therapeutic properties.[18] In this context, derivatives of this architecture incorporating the Ru^{II}(dppn) moiety (dppn = benzo[*i*]dipyrido[3,2-*a*:2',3'-*c*]phenazine), have proven to be excellent $^1O_2$ sensitizers[19] and very promising leads for photodynamic therapy, PDT.[20-22]

Related studies have revealed that Re^{I} complexes - such as $[Re(CO)_3(L)(dppz)]^+$ (L = monodentate pyridyl ligand) - are capable of *directly* photo-damaging DNA.[23-26] However, there are drawbacks to these systems compared to their Ru^{II} analogues: as they are monocations, they possess greatly reduced binding affinity relative to that of the dicationic Ru^{II} complex,[25] furthermore their intraligand ^{3}IL-based emission in water shows a much lower enhancement (>13) upon DNA binding compared to the parent light-switch complex.[24]

The properties of oligonuclear metal complexes for such applications have also been studied as they are expected to bind to larger, or more complex, sites with higher affinities. For example, after the Kelly group demonstrated that two linked non-intercalating $[Ru(bpy)_3]^{2+}$ units displayed appreciable binding to duplex DNA,[27,28] Collins, Keene, and colleagues have investigated a wide range of oligonuclear analogues with differing linker lengths, showing that they bind selectively to non-canonical DNA[29] and RNA structures[3,30] and possess promising antimicrobial properties.[31]

In terms of metallo-intercalators, pioneering studies by Nordén, Lincoln, and co-workers on the synthesis[32] and study[33-35] of dinuclear $[Ru^{II}$(dppz)] systems connected through the dppz ligand showed that although these systems initially groove bind to DNA they ultimately intercalate into duplex DNA through a

threading mechanism.[36-38] However, the construction of such enantiopure architectures from kinetically inert optical isomers can be challenging.

With the aim of constructing more complex oligonuclear architectures,[39,40] the Thomas group has investigated the use achiral mononuclear complexes as building blocks in the "modular" synthesis of non-threading dinuclear metallo-intercalators.[41-44] This approach has, *inter alia*, allowed us to identify Ru[II](dppn)-based systems that are promising leads as sensitizers for PDT[45] and it has also facilitated the construction of an unique heteronuclear complex, **1**[3+] containing both Ru[II](dppz) and Re[I](dppz) units.[46] In our studies on homonuclear Ru[II] systems, we discovered that the nature of the tether ligand employed affects the DNA binding properties of these systems.[44] Therefore - to investigate whether similar effects occur in Ru[II]/Re[I] analogues - we synthesized new complex **2**[3+] and compared it to the originally reported system.
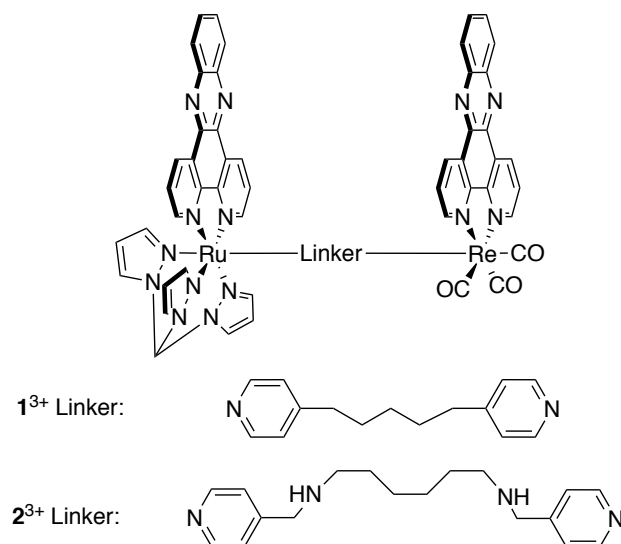
Figure 1. Structure of previously reported[46] complex **1**[3+] and newly synthesized complex **2**[3+] investigated in this study.

Furthermore, as we have recently demonstrated that Ru[II] complexes are eminently compatible with the super-resolution optical microscopy techniques of structured illumination microscopy (SIM) and Stimulated emission depletion microscopy (STED),[47] we investigated the potential of these complexes to function as imaging probes and theranostics. This allowed us to explore the time-dependent uptake of the complexes and provides the first example of tracking subcellular localization dynamics of a probe within live cells at sub-diffraction limits. This work revealed that the photophysics, cellular uptake, localization and even the therapeutic potency of these complexes are profoundly dependent on the nature of the linker used to tether the Ru[II](dppz) and Re[I](dppz) units together.

Results and Discussion

Synthesis and characterization

Complex **1**[3+] was synthesized using a reported method.[46] Similarly, complex **2**[3+] was obtained as its hexafluorophosphate salt from the reaction of two previously reported mononuclear complexes[25,44] using the same procedure employed in the synthesis of **1**[3+] - See SI for details. Analytically pure samples were isolated from repeated anion metathesis and precipitation of its chloride salt in acetone, and then its hexafluorophosphate salt in water.

The UV/Vis absorption spectrum of [**2**](PF$_6$)$_3$ is similar to [**1**](PF$_6$)$_3$ in that it shows high-energy $\pi \rightarrow \pi^*$ transitions, a characteristic structured dppz-based band at ~330 nm, and lower energy [1]MLCT transitions. Excitation into the [1]MLCT of **2**[3+] at 431 nm *or* the dppz-based band results in unstructured luminescence characteristic of the Ru(dπ)$\rightarrow$dppz(π^*) [3]MLCT manifold at 642 nm, demonstrating that, as in **1**[3+], the excited state of the Re[I](dppz) unit is deactivated by non-radiative energy transfer to the lower-lying Ru-based [3]MLCT excited state – see SI. The interaction of [**2**]Cl$_3$ with calf thymus DNA, CT-DNA, in aqueous buffer (25 mM NaCl, 5 m , pH 7.4) was then investigated using UV–visible absorption and luminescence titrations.

Optical studies in the interaction with DNA

On addition of CT-DNA the absorption spectrum of **2**[3+] exhibited changes that are characteristic of DNA binding. Large hypochromicity in both $\pi \rightarrow \pi^*$ and MLCT absorption bands as well as accompanying bathochromic shifts are observed; these changes are typical for an intercalative binding mode.

As expected from many previous studies on M(dppz) complexes, including **1**[3+], complex **2**[3+] is initially non-luminescent in aqueous solutions, but on addition of CT-DNA, its emission is greatly and steadily enhanced, see SI for details. The quantum yields and lifetimes of both complexes in MeCN and when bound to DNA in aqueous solution were also recorded. Given the results of our in-cell studies, *vide infra*, we also investigated the emission of DNA-bound **1**[3+] and **2**[3+] in acidic conditions. As duplex DNA is relatively stable in acid conditions and large-scale structural changes and denaturing of genomic DNA - largely due to protonation of nucleobase steps - are only observed at pH 3.5 and below, [48-50] we recorded this latter data in citrate buffer at pH4, an acidity level found in the lysosome – Table 1.

Table 1 Quantum yields and lifetimes for the emission hexafluorophosphate salts of 1[3+] and 2[3+] in MeCN and their chloride salts when bound to DNA in aqueous buffer at pH7 (Tris buffer) and pH4 (Citrate buffer).

Complex	Solvent	Φ	Lifetime (μs)
1[3+]	MeCN	2.5×10^3	162
	pH7	1.4×10^3	145/33
	pH4	$9. \times 10^4$	167/27
2[3+]	MeCN	2.3×10^3	186
	pH7	2.8×10^3	151/30
	pH4	2.5×10^3	129/24

In MeCN the emission characteristics of the hexafluorphosphate salts of both complexes are quite similar. Both show a single emission lifetime, with **2**[3+] displaying a slightly longer lifetime. However, these lifetimes and associated quantum yields are entirely comparable to those obtained for related complexes containing the Ru[II](tpm)(dppz) fragment that we have previously studied. [43]

The water-soluble chloride salts showed no emission in neutral or acidic conditions until they were bound to DNA. Again, the emission parameters of **1**[3+] and **2**[3+] in these circumstances are very

2

Fitting of the spectral change (emission maximum) to the McGhee-von Hippel model for binding to an isotropic lattice,[51] yielded a K_b of 5.5×10^5 M^{-1}, a value that is almost identical to that observed for 1^{3+}, indicating that – unlike their di-Ru^{II} analogues[44] – the change of linker between the two complexes has little effect on the DNA binding properties of these systems.

As previous cell-free studies on 1^{3+} have demonstrated that it photo-cleaves DNA,[43] similar studies were carried out on complex 2^{3+}. The photocleavage ability of the new complex was assessed using supercoiled pBR 322 plasmid DNA and analyzed by electrophoresis on an agarose gel. Surprisingly, even after prolonged irradiation for up to 60 mins over a range of concentrations (10, 20 and 40 μM) no evidence of photo-cleavage was observed. Despite the fact that the only difference between the 1^{3+} and 2^{3+} is the linking tether, these observations suggest that the Re^I(dppz)-based excited state of 2^{3+} is not sufficiently high in energy, or too short-lived, to produce DNA damage. As it is known that MLCT excited states can be quenched through photo-induced electron transfer processes involving nitrogen lone pairs, [52,53] the photophysics of the two complexes was investigated in more details.

## Time resolved absorption spectroscopy

Ultrafast transient absorption measurements were carried out on the chloride salts of 1^{3+} and 2^{3+} in TRIS buffer with and without CT-DNA (Figure 2).

The excited state spectra of each complex was obtained under 400 nm excitation as previous studies have shown that this populates MLCT states localized on both units.[23,25,44,46] The resultant spectra are dominated by a broad short-lived transient absorption, in the range 500 – 700 nm, which is consistent with the population of a metal→dppz(π^*) ^{3}MLCT state.[54] The bands at ~470 nm and ~600 nm, indicative of dppz-radical anion coordinated to a metal center, are also present;[55] an absorbance at 475 nm has also been reported for a dppz-localised excited state.[56] In the absence of DNA, the transient spectra decay almost to the baseline within several nanoseconds, with the somewhat faster decay occurring for 2^{3+} (τ = 160 ps) than 1^{3+} (τ = 210 ps).

Whilst the detailed photophysical study is not the focus of this work, we note that the transient spectral profile is time-dependent, which is indicative of several excited states being present (Re/phen MLCT, Ru/phen MLCT, and dppz-based excited states) as is typical for metal complexes of the dppz-ligand.[56] Whilst these excited states undergo ultrafast decay in water, with the addition of DNA, the spectra do not decay to the baseline within the instrument-limited duration of the experiment (7900 ps). This difference is consistent with the DNA "light switch" effect common to {Ru(dppz)} species, as well as the observed increase in luminescence for these complexes upon binding to DNA.[57]

In the presence of DNA 1^{3+} exhibits distinctive spectral features at 600 nm, and 550 and 475 nm, which are comparable with the early- and late-time spectra of the complex respectively in the absence of DNA. The absorptions >600 nm are much more

pronounced then in the case of 2^{3+} (Fig. 2B and 2D). The difference in the spectral profiles is a strong indication that photoinduced reactions of **1** and **2** with the DNA are affected by the nature of the linker. To gain insight into the electronic structure of these compounds and their differences, quantum based DFT calculations were performed.
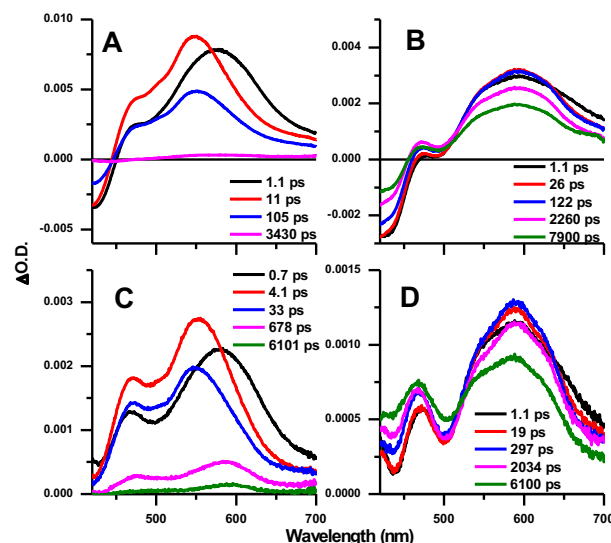
Figure 2. Transient absorption spectra at selected time delays, 5 μM complex or 5 μM complex:25 μM bp^{-1} CT-DNA A) 2^{3+} in TRIS buffer B) 2^{3+} in TRIS buffer with CT-DNA C) 1^{3+} in TRIS buffer D) 1^{3+} in TRIS buffer with CT-DNA.

Computational Studies

All calculations were performed using Gaussian09, version D.01[58] using B3LYP/GD3BJ [59,60] using the procedure outlined in the Supporting information, focusing on their behavior in solution without any DNA present. Calculations performed for a variety of conformers led to the lowest energy singlet (S_0) and triplet (T_1) states for 1^{3+} and 2^{3+}. This analysis also included analogous calculations where four water molecules were explicitly included, which we label $1w^{3+}$ and $2w^{3+}$. The results of this analysis are summarized in Figure 3. Overlays of the singlet and triplet states for 1^{3+} and 2^{3+} are given in the supporting information (Figure S11 and S12), where we also show the overlap between the lowest energy singlet isomer of $1w^{3+}$ and $2w^{3+}$ and their first triplet state (Figure S13 and S14).

The overlays show that, in each individual case, these conformers are structurally very similar. However, it is clear from Figure 3 that there are a number of qualitative differences between 1^{3+} and 2^{3+}; differences that are largely retained in a parallel comparison of $1w^{3+}$ and $2w^{3+}$. First, while the two dppz units of both 1^{3+} and 2^{3+} approach co-planarity, due to the differences in linker length, they are close to parallel in 1^{3+}/$1w^{3+}$ but almost orthogonal to each other in 2^{3+}/$2w^{3+}$. This has consequences for both adsorption and emission spectra, as transition dipole moments involving dppz will be mutually amplified in the structure of 1^{3+}/$1w^{3+}$, but this will be more difficult in the case of 2^{3+}/$2w^{3+}$.

A second structural difference is that in the case of 1^{3+} the Ru-dppz moiety is closer in space to the flexible linker moiety of the bridging ligand than the Re-dppz, whereas for 2^{3+} that situation is reversed. The inclusion of water molecules results in the Re-dppz moiety being closest to the linker in both $1w^{3+}$ and $2w^{3+}$.

3
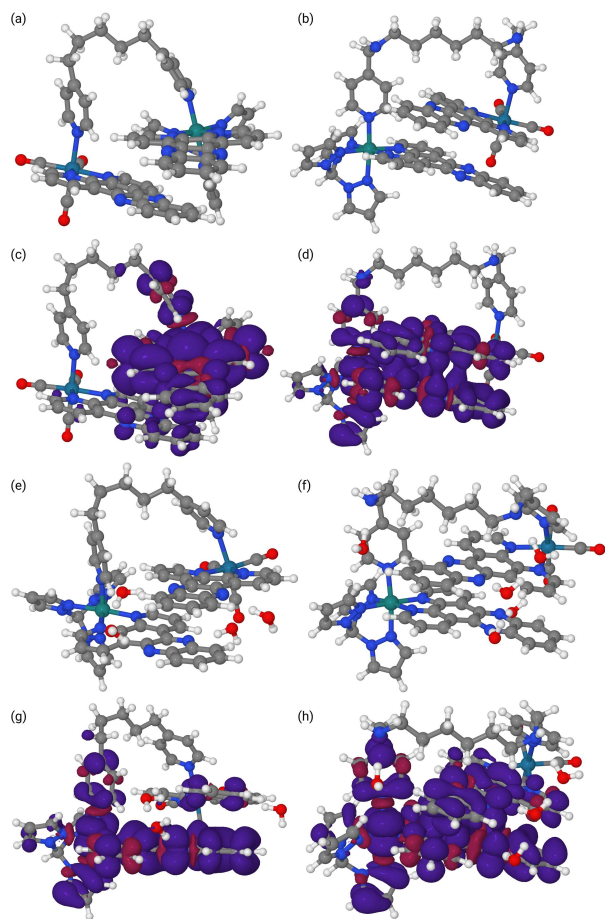
Figure 3: Calculated structures for the lowest singlet and triplet states for $\mathbf{1}^{3+}$, $\mathbf{2}^{3+}$, $\mathbf{1w}^{3+}$ and $\mathbf{2w}^{3+}$. Panel (a): $\mathbf{1}^{3+}$ (S_0). Panel (b): $\mathbf{2}^{3+}$(S_0). Panel (c): $\mathbf{1}^{3+}$(T_1) with spin density (isosurface at 0.0004 with α spin purple and β spin red) superimposed. Panel (d): $\mathbf{2}^{3+}$(T_1) with spin density (isosurface at 0.0004 with α spin purple and β spin red) superimposed. Panel (e): $\mathbf{1w}^{3+}$ (S_0). Panel (f): $\mathbf{2w}^{3+}$(S_0). Panel (g): $\mathbf{1w}^{3+}$(T_1) with spin density (isosurface at 0.0004 with α spin purple and β spin red) superimposed. Panel (h): $\mathbf{2w}^{3+}$(T_1) with spin density (isosurface at 0.0004 with α spin purple and β spin red) superimposed.

A final difference between the two structures is that the pyridyl-group of the tether ligand coordinated to the Re center has a different orientation in $\mathbf{1}^{3+}$ compared to $\mathbf{2}^{3+}$, again this feature is maintained in the structures of $\mathbf{1w}^{3+}$ and $\mathbf{2w}^{3+}$. Due to computational time restraints an exhaustive conformational search was not possible; so - to ensure that fortuitous sampling did not cause these findings - the position of the metal centers and ancillary ligands for $\mathbf{1}^{3+}$, $\mathbf{2}^{3+}$, $\mathbf{1w}^{3+}$, and $\mathbf{2w}^{3+}$ were inverted and re-optimized. In both cases, this resulted in energies that were higher than for the situation depicted in Fig 3 (See SI for final structures). How the structural differences discussed above might affect photo-excited states of the two complexes in water (without any DNA present) was then computationally investigated.

Comparisons between the simulated UV-VIS spectra for $\mathbf{1}^{3+}$ and $\mathbf{2}^{3+}$ on the one hand and $\mathbf{1w}^{3+}$ and $\mathbf{2w}^{3+}$ on the other hand shows that, overall, they are all remarkably similar (Figures S15 and S16, SI). However, a detailed wave function analysis using the TheoDORE program[61] is more revealing. Whilst the range of oscillator strengths between $\mathbf{1}^{3+}$ and $\mathbf{2}^{3+}$ is quite similar, the character of the transitions is very different, as is clear from Figures

S17 and S18 in the SI. Similar images are also provided for $\mathbf{1w}^{3+}$ and $\mathbf{2w}^{3+}$ in Figures S19 and S20. Two particular aspects are worth highlighting.

First, for $\mathbf{1}^{3+}$, the ^{1}MLCT excitations at low energy are mainly due to charge transfer from the Ru center onto both dppz moieties and its π-π* transitions also involve vertical and cross-excitations transitions to and from both dppz moieties. Although $\mathbf{2}^{3+}$ displays similar π-π* transitions, its strongest ^{1}MLCT transitions are largely restricted to the Ru-dppz moiety. Secondly, the linker for $\mathbf{1}^{3+}$ is not involved in any of the strong transitions ($f > 0.01$), whereas in the case of $\mathbf{2}^{3+}$ the linker is involved - either as a source or as a destination of the excitation. This suggests that for $\mathbf{2}^{3+}$ the character of the amino-groups in the linker can change dramatically after excitation, altering the photochemical behavior in biological systems. This is supported by our calculations on $\mathbf{1w}^{3+}$ and $\mathbf{2w}^{3+}$, where there are more transitions involving the linker for $\mathbf{2w}^{3+}$ than for $\mathbf{2}^{3+}$; it is also clear that the oscillator strengths for $\mathbf{1w}^{3+}$ and $\mathbf{2w}^{3+}$ are lower on the whole than for the case without coordinated water.

Finally, the nature of the emission from the triplet state was considered. As is clear from Fig. 3 (panels (c) and (d)) the spin density of the first triplet state of $\mathbf{1}^{3+}$ and $\mathbf{2}^{3+}$is dramatically different. In $\mathbf{1}^{3+}$ it is largely centered on the Ru-dppz, whereas for $\mathbf{2}^{3+}$ it is spread over both dppz units. The same is the case for $\mathbf{1w}^{3+}$ and $\mathbf{2w}^{3+}$ as is clear from panels (g) and (h). The emission wavelengths for $\mathbf{1}^{3+}$ and $\mathbf{2}^{3+}$ (as a 0-0 transition) are calculated to be 667 and 725 nm, respectively, and the equivalent figures for $\mathbf{1w}^{3+}$ and $\mathbf{2w}^{3+}$ are 748 and 785 nm.

The spread of the wave function over both dppz units results in a red-shift of the emission wavelength for $\mathbf{2}^{3+}$/$\mathbf{2w}^{3+}$, which is to be expected. For both $\mathbf{2}^{3+}$ and $\mathbf{2w}^{3+}$ the calculated wavelength is longer than experimental figure. Most likely this is because that in these initial calculations conformational motion of the molecule, is not taken into account, although future calculation may also require a more complete solvation shell to describe this transition. Certainly, calculations on an extended structure for $\mathbf{2}^{3+}$ shows that emission wavelength shifts to 652 nm (696 nm for $\mathbf{2w}^{3+}$), giving credence to the hypothesis that geometrical motion play a role in the energy of the excited state. However, the lowest singlet and triplet structures for this extended structure are calculated to be 91 kJ mol^{-1} and 111 kJ mol^{-1} higher in free energy than the those for the structure in Figure 3(b), making it unlikely for these specific structures contribute to the conformers in solution. For all conformers of the extended structures of $\mathbf{1}^{3+}$ and $\mathbf{2}^{3+}$ studied (with or without water coordinated), the two metal centers are essentially decoupled (see Figures S21-S24), although some strong cross-ligand excitations from Ru to the Re-moiety are still present. A similar comparison of energies with $\mathbf{2w}^{3+}$ is more difficult. A minimum number of water molecules needed to describe the solvation shell of each conformation of $\mathbf{2w}^{3+}$ without biasing the results was chosen; consequently this number differs for the extended and closed conformers, meaning that any direct comparison of their energetics would be non-trivial.

Although an exhaustive conformational search was beyond the scope of this study, the completed calculations echo the spectroscopic experiments and provide insights into why the photophysical properties of $\mathbf{1}^{3+}$ and $\mathbf{2}^{3+}$ are affected by their linking ligand and illustrate how the nature and conformation of the tether moiety have profound effects on the excited state of these linked systems. Given the flexibility of both tethers, the folded and

extended structures described herein are probably limiting forms of a range of dynamic conformers in solution although the calculations clearly indicate that structures with co-planar dppz units will be energetically preferred, at least in simple solutions.

As no cell-based studies on heterometallic Ru/Re dppz complexes have as yet been reported, the cytological properties of 1^{3+} and 2^{3+} were then investigated.

Cell studies

Initially the cytotoxicity of both 1^{3+} and 2^{3+} were determined over a range of concentrations (1-200 μM) to obtain 48 hour IC_{50} values against both the A2780 cisplatin sensitive cell line and the cisplatin resistant variant A2780cis cell lines (Table 2).

Table 2 IC_{50} (μM) values for A2780 and A2780cis cells treated with complexes 1^{3+} and 2^{3+}

Cell line	48 hr IC_{50} con. (μM)		
	1^{3+}	2^{3+}	cisplatin
A2780	79	11	2
A2780cis	>200	21	22

The IC_{50} for 1^{3+} against A2780 cells was determined to be 79 μM, indicating that this complex is considerably less potent than cisplatin (IC_{50} = 2 μM) under the same conditions. Indeed, despite the expected drop in activity against the resistant A2780cis line (IC_{50} = 22 μM), cisplatin is still much more potent than complex 1^{3+}, which also displays a large decrease in activity against this line.

Surprisingly, complex 2^{3+}, displays appreciably higher cytotoxicity against A2780 cells than 1^{3+} and is equipotent with cisplatin against A2780cis cell line. These data also reveal that the Resistance Factor (RF = IC_{50}(A2780)/IC_{50}(A2780cis) for 2^{3+} (RF <2) is much lower than cisplatin (RF = 11), indicating a lack of cross-resistance with the platinum-based therapeutic.

Although complex 2^{3+} does not cleave DNA in cell-free conditions, the in-cell phototoxic activity of both complexes against the two cell lines was investigated using a previously published protocol. Again surprisingly, the phototoxicity of both complexes was minimal. At irradiation of 48 J cm^{-2}, the phototoxic indices of complexes 1^{3+} and 2^{3+} were determined as ~1.2 and 2 respectively (See SI). For complex 2^{3+} these findings are consistent with the lack of DNA cleavage reported in the previous section. However, as 1^{3+} is capable of photocleaving DNA in cell-free studies, the lack of phototoxicity is somewhat unexpected. To investigate this issue in more detail further experiments on the uptake of the complexes were carried out. Given that complexes 1^{3+} and 2^{3+} display off-on switching effects and do not display greatly enhanced phototoxicity we initially exploited their emission properties by resolution-limited microscopy.

Treatment of A2780 cells with either 1^{3+} or 2^{3+} leads to staining; however, the details of the staining patters are strikingly different. Luminescence imaging using widefield microscopy revealed that, at all concentrations, complex 1^{3+} only displays emission from the nucleus. Although the complex could also be imaged using the super-resolution technique structured illumination microscopy, SIM, Figure 4, it exhibits rapid photobleaching, which hampered further imaging studies. Contrastingly, 2^{3+} displays negligible photobleaching when imaged in cells and its intracellular localization is concentration-dependent. At concentrations below its IC_{50} value, the intracellular emission of 2^{3+} appears punctated and only present in the cytosol. However, at higher concentrations - particularly above the IC_{50} - distinct nuclear staining is also observed.
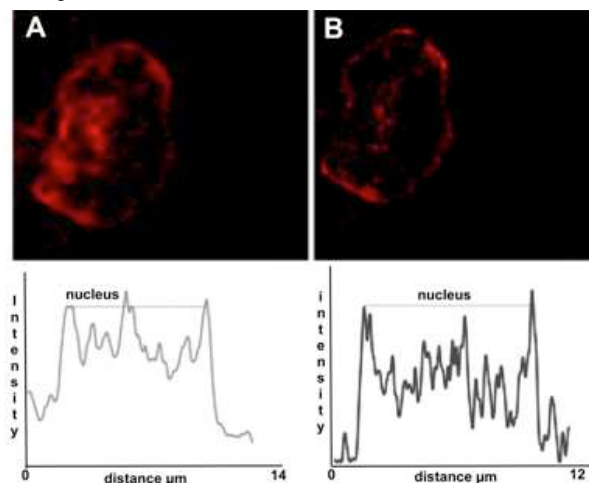
Figure 4. Comparative widefield (A) and SIM (B) images of A2780 cells stained with complex 1^{3+} (100 μM) with corresponding intensity line profile shown below the image.

We have recently demonstrated that a photostable dinuclear Ru^{II} complex containing a rigid planar bridging ligand is an excellent probe for not only SIM but a second super resolution technique, STED microscopy.[47] STED is particularly attractive as it can theoretically attain infinitely high resolution and experimental resolutions of ≤50 nm are frequently obtained.[62-64] However, selective deactivation of the photo-excited probe through a depletion beam requires luminophores with highly photostable excited states.[65] The lack of photobleaching of 2^{3+} prompted us to explore whether its overall optical properties were compatible with demands of STED protocols. Using high-resolution HyVolution, deconvoluted laser scanning confocal microscopy (d-LSCM) - which in itself doubles lateral resolution compared to conventional confocal methods – and deconvoluted STED (d-STED) (using a 775 nm depletion beam into the low energy edge of the ^{3}MLCT band) the punctated emission produced by 2^{3+} within cells at low treatment concentrations was investigated by co-staining with commercial lysotracker and mitotracker probes. – Figure 5. The increased sensitivity of STED facilitated these experiments and illustrated the power of this technique over conventional methods.

5
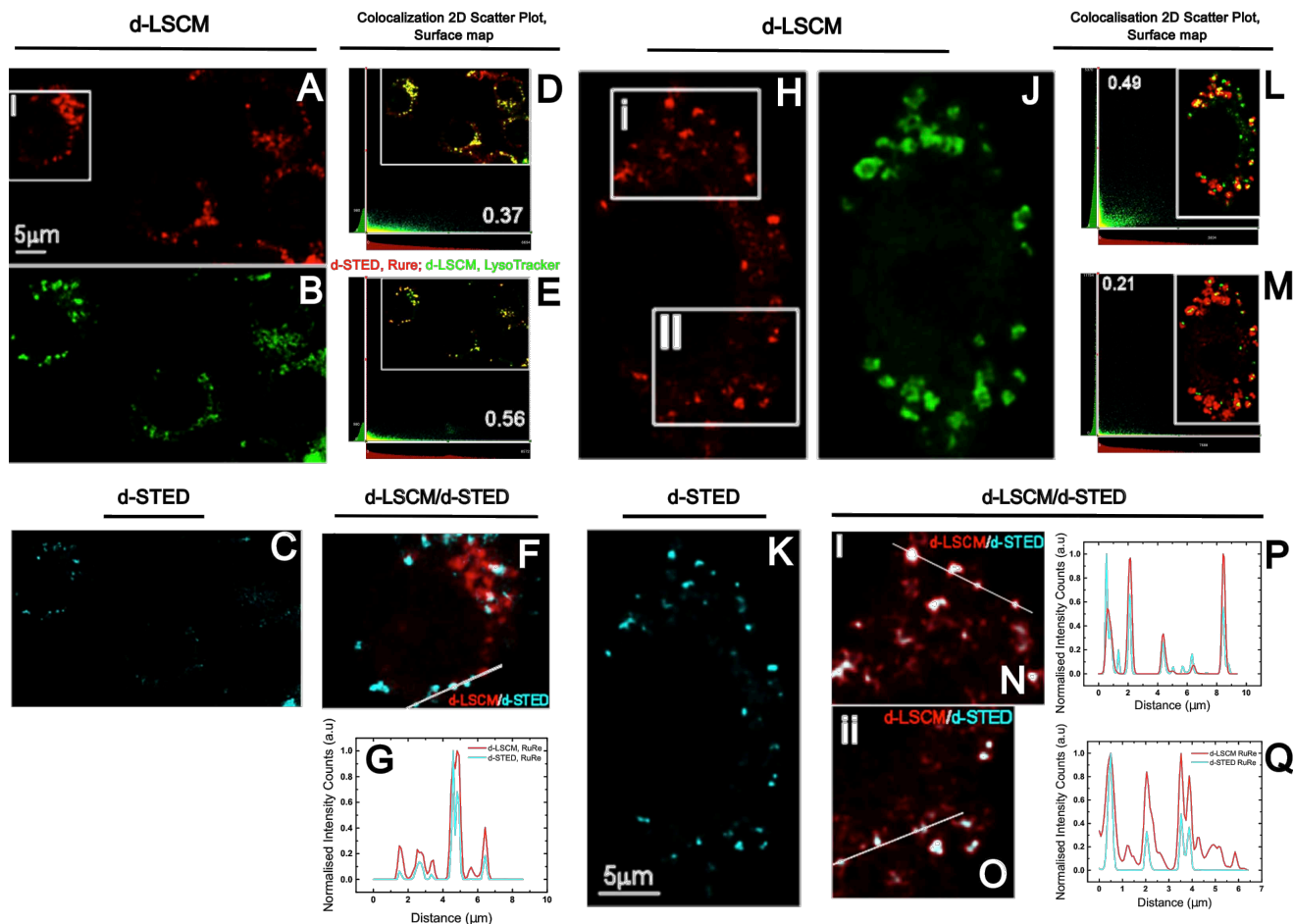
Figure 5. Super resolution deconvoluted Stimulated Emission Depletion (d-STED) nanoscopy of MCF-7 cells compared to deconvoluted Laser Scanning Confocal Microscopy (d-LSCM) using Leica HyVolution employing 0.5 airy units pinhole aperture. Images A-B: Lysosomal staining at 6 μM [**2**]Cl$_3$, deconvoluted images shown in red (A), Lysotracker in Green (B), and [**2**]Cl$_3$ STED in cyan (C). Merged d-LSCM images of [**2**]Cl$_3$ in red and Lysotracker in green are shown in the white-framed inset colocalization maps, displaying the colocalized objects in yellow (D); 2D scatter plot of the pixel colocalisation distribution, and calculated Pearson's coefficients (D). Merged images of d-STED of [**2**]Cl$_3$ in Red, and d-LSCM of Lysotracker in green are shown in the white-framed inset colocalization maps, displaying the colocalised objects in yellow (E); scatter plot of the pixel colocalisation distribution, and calculated Pearson's coefficients (E). Merged images of d-LSCM in red and d-STED of [**2**]Cl$_3$ in cyan are shown (F); normalised intensity line profile is shown in (G) of the white line drawn in (F); enhancement of the resolution by d-STED can be observed in the compared-merged images, as well as in the full-width-half-maximum (FWHM) of the line profile. Images H-K: Deconvoluted images of mitochondrial staining with 6 μM [**2**]Cl$_3$, of RuRe shown in red (H), Mitotracker in Green (J), and [**2**]Cl$_3$, STED in cyan (K). Merged d-LSCM images of [**2**]Cl$_3$, in green and Mitotracker in red are shown in the white-framed inset colocalization maps, displaying the colocalised objects in yellow (L); 2D scatter plot of the pixel colocalisation distribution, and calculated Pearson's coefficients (L). Merged images of d-STED of [**2**]Cl$_3$, in green, and d-LSCM of Mitotracker in red are shown in the white-framed inset colocalization maps, displaying the colocalised objects in yellow (M); scatter plot of the pixel colocalisation distribution, and calculated Pearson's coefficients (M). White squared insets in (H), are magnified in (i, ii); merged images of [**2**]Cl$_3$, on d-LSCM in red and on d-STED in cyan are shown (N and O); normalised intensity line profile of the white line drawn in (N) is shown in (P); normalised intensity line profile of the white line drawn in (O) is shown in (Q); enhancement of the resolution by d-STED can be observed in the compared-merged images, as well as in the FWHM of both line profiles

Both the high- and super-resolution studies confirmed that the complex localizes in lysosomes and mitochondria, however there were some interesting differences in the results. Analysis of the d-LSCM data for the co-localization of **2**$^{3+}$ led to a Pearson coefficient of 0.37 with lysotracker and 0.49 with mitotracker – Fig 5D and E. However, when the analyses were carried out on the same cells using the substantially higher resolutions available through STED, Fig 5L and M, these figures changed to 0.56 and 0.21 respectively indicating that emission is largely observed within lysosomes rather than mitochondria.

As described above, in cell-free conditions **2**$^{3+}$ only displays emission in neutral and acidic solution found in a lysosome when bound to DNA, suggesting the complex is not freely solvated in the lysosomal compartment. Although it is now known that lysosomes can contain nucleic acids through direct uptake mechanisms[66,67], it is well-established that light-switch complexes are also switch on in many other lipophilic environments[68-71] including lipid-rich regions[72]. The fact that emission is seen from lysosomes and mitochondria suggest the complex is bound in such environments.

6
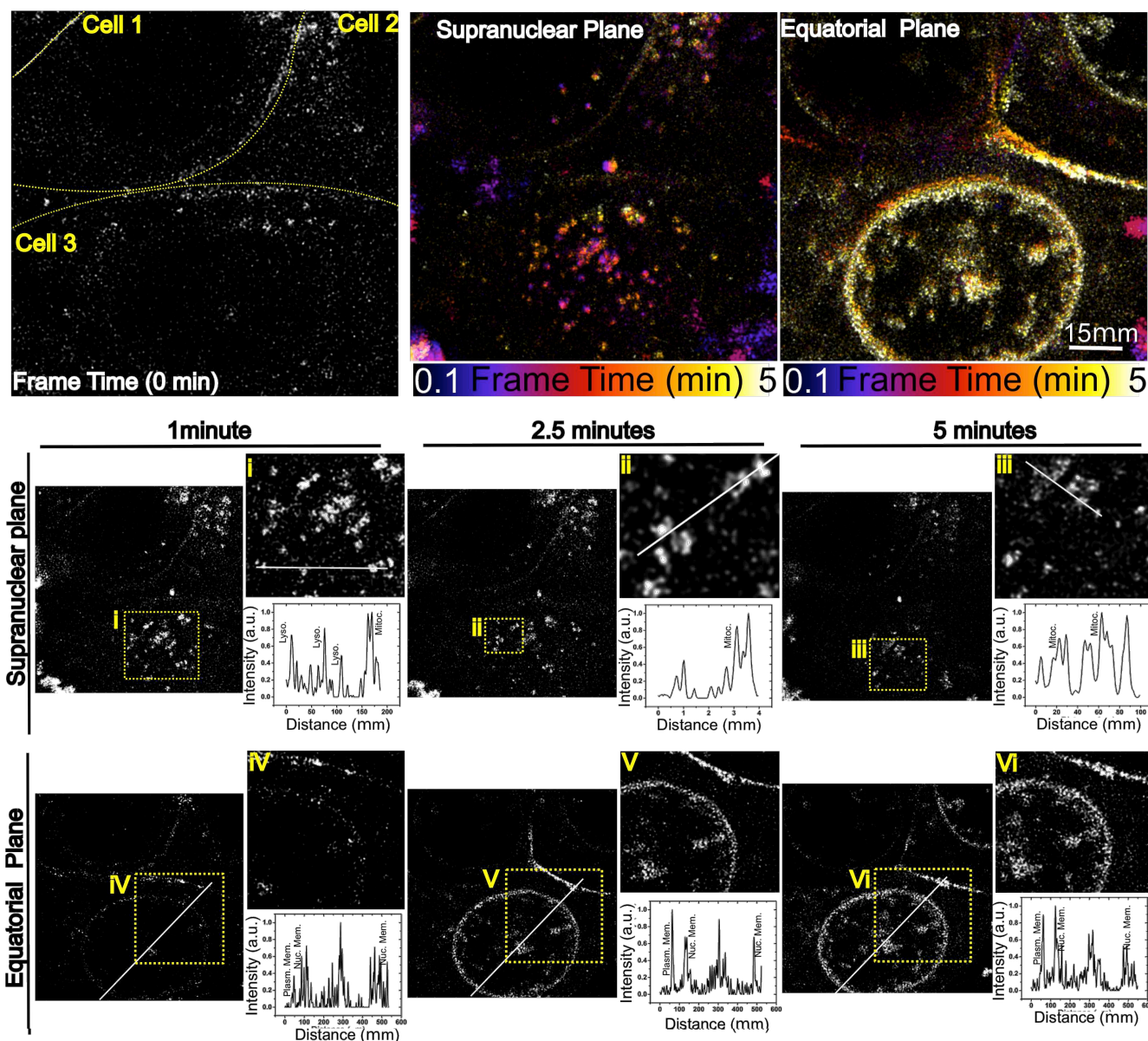
Figure 6. Kymographs showing time dependent cell permeation and localization of [**2**]Cl₃ in MCF7 cells at different intracellular focal planes imaged through d-STED. Uppermost left-hand side: top image show three MCF-7 cells stained with 500 μM **2**³⁺ before starting the time-lapse imaging. The red dashed region of interest (ROI) is zoomed-in and displayed to the right hand side. The middle image shows the supranuclear plane of the ROI. The false colours observed correspond to the time-lapse evolution of the cellular components; as displayed in the scale below. First time points are shown in blue and the last time points in light yellow. This 2D kymograph representation over 5 minutes reveals the evolution of lysosomes and mitochondria imaging, as well as the plasma membrane. The top uttermost right-hand sided image shows the same ROI but at a different z-axial position, the nuclear equatorial plane. Similarly, the 2D kymograph representation over 5 minutes allows tracking **2**³⁺; nuclear staining, over lysosomes and mitochondria localization, becomes more apparent towards the end of imaging time period,. Below, the ROIs of the two different planes investigated are shown after 1min, 2.5 and 5 minutes of time-lapses. From each image a yellow dashed square inset is zoomed-in and shown at its right-hand side (i,ii,iii,iv,v,vi) , where super-resolved image of the lysosomes, mitochondria, plasma membrane and nuclear membrane are shown; the white line in each image corresponds to the accompanying normalised intensity profile .

Although these data confirm that emission from **2**³⁺ is from the two organelles, the quantitative differences between LSCM and STED indicate that higher resolution technique more successfully deconvolutes the optical signals of **2**³⁺ and the two commercial probes. As mentioned above, at exposures to **2**³⁺, above its IC₅₀ concentration nuclear staining was observed. This was confirmed by co-localization experiments. For example, at 500 nm concentrations, cells co-stained with the nuclear DNA stain Hoechst 33342 and imaged by widefield or super resolution techniques led to Pearson co-localization coefficients of >0.92 – See SI. Thanks to the

photo-stability of **2**³⁺, on exposure to the complex at these concentrations the change in localization could be observed and visualized at STED resolutions in real time.

Images taken immediately after exposure to the complex in the same concentrations used in co-staining experiments show that emission from **2**³⁺ initially localizes in mitochondria and lysosomes of live cells. But its characteristically bright luminescence rapidly migrates, with strong staining of the nucleus and particularly the nuclear membrane developing within five minutes, see Figure 6 for representative kymographs. The dynamics of this processes in both

7

the supranuclear and equatorial planes are strikingly revealed in accompanying STED-based videos – see SI. As far as we aware this is the first time the temporal dynamics of optical probe uptake by live cells have been visualized at super resolutions.

Although the intracellular luminescence of 1^{3+} and 2^{3+} confirms their uptake by live cells, this data is not quantitative, particularly as these complexes display a light-switch effect and thus only emit from lipophilic environments. To obtain a more complete understanding of this issue, inductively coupled plasma mass spectrometry (ICP-MS) was used to determine cellular accumulation of the two complexes in A2780 cells.

After exposure of cells to 1^{3+} and 2^{3+}, the fractionated ruthenium content in both nuclei and cytoplasm were determined. These data, which are summarized in Figure 7A, reveal that live cells take up complex 2^{3+} at appreciably higher levels than 1^{3+}. Furthermore, at this exposure level, whilst both complexes accumulate preferentially within the nucleus, it seems 2^{3+} displays proportionally higher nuclear targeting, as the concentration distribution ratio between the nucleus and cytoplasm is 4.8:1 for 1^{3+} and 5.4:1 for 2^{3+} respectively, Due to the combination of increased overall uptake and nuclear targeting, accumulations of 2^{3+} within the nucleus is almost x2.5 times higher than that of 1^{3+}.
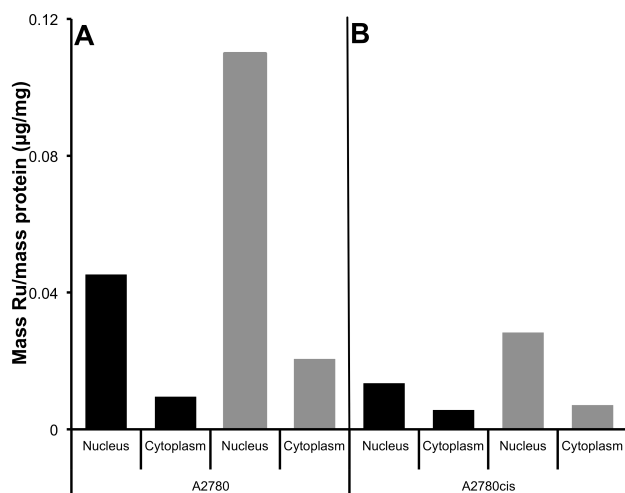
Figure 7. ICP-MS data for the uptake of 1^{3+} (■) and 2^{3+} (▨) in (A) A2780 cells and (B) A2780cis cells

The increase in intracellular concentration and nuclear targeting of 2^{3+} suggests cell uptake causes the enhanced cytotoxicity of this complex relative to 1^{3+}. This hypothesis was further explored through analogous experiments with A2780cis cells.

Previous studies have established that therapeutic resistance of A2780cis to cisplatin is due to more than one mechanism.[73,74] Although it is known that mismatch repair mechanisms are repressed, one of the main resistance mechanisms in this cell line involves decreased expression of the CTR1 copper transporter protein, resulting in a lowered intracellular concentrations of cisplatin.[75]

Therefore, to investigate whether the reduction in potency of 1^{3+} and 2^{3+} against A2780cis cells is also associated with changes in the intracellular accumulation of the complexes, ICP-MS studies on this line were also carried out – Fig 7B.

Using identical conditions to those employed for the A2780 study, it was found that there was a considerable decrease in intracellular accumulation of the complexes within A2780cis cells. Although live cell uptake of complex 2^{3+} is again appreciably higher

than 1^{3+} by a factor of ~2.5, accumulation of both complexes is considerably lower than in the A2780 line. For example, nuclear uptake of 2^{3+} within A2780 cells is × 4 higher than in A2780cis cells.

Conclusions

For the first time, the cellular properties of mixed metal oligonuclear Ru/Re-dppz-based complexes and the effects of linking ligand on the cell uptake properties of dinuclear metallointercalators has been explored. In our original work on related homonuclear Ru^{II}-systems, the linker employed in 2^{3+} was chosen for its potential to mimic polyamines such as spermine and spermidine. These ubiquitous biomolecules not only display non-specific binding to nucleic acids through electrostatic interactions, but are also established vectors for nuclear delivery.

The comparison between 1^{3+} and 2^{3+} indicates that the linker does indeed improve cellular delivery and nuclear targeting. Somewhat unexpectedly the ultrafast transient absorption studies reveal that the linker also affects the photophysical properties of 2^{3+}, decreasing the relative population of a high-energy Re^{I}(dppz)-localized $\pi/n \rightarrow \pi^*$ state upon excitation. These observations explain the low phototoxicity of 2^{3+} and its inability to photo-damage DNA in cell-free conditions. The changes in excited state properties also accounts for the low in-cell photobleaching properties of 2^{3+}. Contrastingly, the rapid bleaching of 1^{3+} explains its lack of photo-toxicity in live cells, even though it damages DNA in cell-free conditions.

The enhanced uptake and nuclear delivery of 2^{3+} afforded by its tether only partially explains its increased cytotoxicity when compared to 1^{3+}. For example, a comparison of the ICP-MS data for A2780 and A2780cis cells show that despite the decreased uptake of both 1^{3+} and 2^{3+} in A2780cis cells, 2^{3+} largely retains its cytotoxicity and is thus potent at concentrations that are a order of magnitude lower than 1^{3+} in the same cell line. This observation suggests that the enhanced potency of 2^{3+} compared to 1^{3+} may not solely be due to differences in uptake but may be a consequence of changes in biomolecular targeting properties. Studies to investigate this issue in more detail will form the basis of future reports. It should also be noted that the homonuclear Ru^{II} analogues of 1^{3+} and 2^{3+} are photo-stable but not classically cytotoxic.[45] Therefore, it seems the distinctive properties of 1^{3+} and 2^{3+} may also be attributed to the substitution of a $[Ru(dppz)]^{2+}$ unit with a $[Re(dppz)]^+$ moiety.

Finally, it is known that polyamines are readily protonated in cellular conditions. Although no changes in emission characteristics across cells is observed, the preferential localization of 2^{3+} within lysosomes hints that – at least in the acidic conditions found within these organelles - the amine sites within its tether may protonate, yielding a more cationic form. This increased polarity would disfavor trans-membrane diffusion out of the organelle. Consequently, studies to investigate the effect of pH on the physiochemical and photophysical properties of this complex are underway.

In summary, we have identified a heterometallic metallointercalator that displays good uptake into the nuclei of live cells, where it can be used as a probe for STED imaging protocols; the complex also displays promising cytotoxicity in a therapeutically resistant cancer line. Taken together, these properties mean that the new complex is an attractive lead for the construction of new theranostics compatible with super-resolution imaging. Derivatives that enhance the imaging capabilities and/or therapeutic activity of this prototype system are currently being constructed.

ASSOCIATED CONTENT

SUPPORTING INFORMATION

Experimental details, DNA titrations, additional transient absorption data, Cleavage gels, microscopic slide preparation/protocols additional images and colocalization studies, ICP-MS protocol and whole cell figures, details of cytotoxicity and phototoxcity studies, and STED-based videos showing uptake of [**2**]Cl$_4$ at high exposure. In addition, the SI contains all computational details as well as coordinates of the final geometries of the optimizations. Additional references[67-76] are referenced in the SI.

AUTHOR INFORMATION

Corresponding Authors

* j.bernardino-de-la-serna@imperial.ac.uk
* james.thomas@sheffield.ac.uk

Present Addresses

▲ The Daniel K. Inouye College of Pharmacy, University of Hawai'i at Hilo, 200 W. Kawili Street, Hilo, HI 96720-4091.
◆ CRUK/MRC Oxford Institute for Radiation Oncology, Department of Oncology, University of Oxford, Oxford OX3 7DQ, UK.

ACKNOWLEDGMENT

REFERENCES

(1) Erkkila, K. E.; Odom, D. T.; Barton, J. K. *Chem. Rev.* **1999**, *99* (9), 2777.

(2) Metcalfe, C.; Thomas, J. A. *Chem Soc Rev* **2003**, *32* (4), 215.

(3) Keene, F. R.; Smith, J. A.; Collins, J. G. *Coord. Chem. Rev.* **2009**, *253* (15-16), 2021.

(4) McKinley, A. W.; Lincoln, P.; Tuite, E. M. *Coord Chem Rev* **2011**, *255* (21-22), 2676.

(5) Gill, M. R.; Thomas, J. A. *Chem Soc Rev* **2012**, *41* (8), 3179.

(6) Komor, A. C.; Barton, J. K. *Chem. Commun.* **2013**, *49* (35), 3617.

(7) Qiu, K.; Chen, Y.; Rees, T. W.; Ji, L.; Chao, H. *Coord Chem Rev* **2017**, 1.

(8) Poynton, F. E.; Bright, S. A.; Blasco, S.; Williams, D. C.; Kelly, J. M.; Gunnlaugsson, T. *Chem Soc Rev* **2017**, *36*, 1.

(9) Friedman, A. E.; Chambron, J. C.; Sauvage, J. P.; Turro, N. J.; Barton, J. K. *J. Am. Chem. Soc.* **1990**, *112* (12), 4960.

(10) Puckett, C. A.; Barton, J. K. *J. Am. Chem. Soc.* **2007**, *129* (1), 46.

(11) Zhu, B.-Z.; Chao, X.-J.; Huang, C.-H.; Li, Y. *Chem. Sci.* **2016**, *7* (7), 4016.

(12) Mari, C.; Pierroz, V.; Ferrari, S.; Gasser, G. *Chem. Sci.* **2015**, *6* (5), 2660.

(13) Zeng, L.; Gupta, P.; Chen, Y.; Wang, E.; Ji, L.; Chao, H.; Chen, Z.-S. *Chem Soc Rev* **2017**, *46* (19), 5771.

(14) Heinemann, F.; Karges, J.; Gasser, G. *Acc. Chem. Res.* **2017**, *50* (11), 2727.

(15) Sentagne, C. C.; Chambron, J. C. J.; Sauvage, J. P. J.; Paillous, N. N. *J Photochem Photobiol B* **1994**, *26* (2), 165.

(16) Ortmans, I. I.; Elias, B. B.; Kelly, J. M. J.; Moucheron, C. C.; Kirsch-DeMesmaeker, A. A. *Dalton Trans* **2004**, No. 4, 668.

(17) Burke, C. S.; Byrne, A.; Keyes, T. E. *J. Am. Chem. Soc.* **2018**, *140* (22), 6945.

(18) Mari, C.; Pierroz, V.; Rubbiani, R.; Patra, M.; Hess, J.; Spingler, B.; Oehninger, L.; Schur, J.; Ott, I.; Salassa, L.; Ferrari, S.; Gasser, G. *Chem. Eur. J.* **2014**, *20* (44), 14421.

(19) Foxon, S. P.; Alamiry, M. A. H.; Walker, M. G.; Meijer, A. J. H. M.; Sazanovich, I. V.; Weinstein, J. A.; Thomas, J. A. *J. Phys. Chem. A* **2009**, *113* (46), 12754.

(20) Sun, Y.; Joyce, L. E.; Dickson, N. M.; Turro, C. *Chem. Commun.* **2010**, *46* (14), 2426.

(21) Albani, B. A.; Peña, B.; Leed, N. A.; de Paula, N. A. B. G.; Pavani, C.; Baptista, M. S.; Dunbar, K. R.; Turro, C. *J. Am. Chem. Soc.* **2014**, *136* (49), 17095.

(22) Knoll, J. D.; Albani, B. A.; Turro, C. *Chem. Commun.* **2015**, *51* (42), 8777.

(23) Yam, V.; Lo, K.; Cheung, K. K.; Kong, R. *J. Chem. Soc., Chem. Commun.* **1995**, *0* (11), 1191.

(24) Stoeffler, H. D.; Thornton, N. B.; Temkin, S. L.; Schanze, K. S. *J. Am. Chem. Soc.* **1995**, *117* (27), 7119.

(25) Yam, V. W.-W.; Lo, K. K.-W.; Cheung, K.-K.; Kong, R. Y.-C. *J. Chem. Soc., Dalton Trans.* **1997**, No. 12, 2067.

(26) Olmon, E. D.; Sontz, P. A.; Blanco-Rodríguez, A. M.; Towrie, M.; Clark, I. P.; Vlček, A., Jr.; Barton, J. K. *J. Am. Chem. Soc.* **2011**, *133* (34), 13718.

(27) O'Reilly, F.; Kelly, J.; Kirsch-DeMesmaeker, A. *Chem. Commun.* **1996**, No. 9, 1013.

(28) O'Reilly, F. M.; Kelly, J. M. *J. Phys. Chem. B* **2000**, *104* (30), 7206.

(29) Morgan, J. L.; Spillane, C. B.; Smith, J. A.; Buck, D. P.; Collins, J. G.; Keene, F. R. *Dalton Trans* **2007**, No. 38, 4333.

(30) Gorle, A. K.; Li, X.; Ainsworth, T. D.; Heimann, K.; Woodward, C. E.; Collins, J. G.; Keene, F. R. *Dalton Trans* **2015**, *44* (8), 3594.

(31) Li, F.; Collins, J. G.; Keene, F. R. *Chem Soc Rev* **2015**, *44* (8), 2529.

(32) Lincoln, P.; Nordén, B. *Chem. Commun.* **1996**, No. 18, 2145.

(33) Önfelt, B.; Lincoln, P.; Nordén, B. *J. Am. Chem. Soc.* **1999**, *121* (46), 10846.

(34) Önfelt, B.; Lincoln, P.; Nordén, B. *J. Am. Chem. Soc.* **2001**, *123* (16), 3630.

(35) Wilhelmsson, L. M.; Westerlund, F.; Lincoln, P.; Nordén, B. *J. Am. Chem. Soc.* **2002**, *124* (41), 12092.

(36) Nordell, P.; Lincoln, P. *J. Am. Chem. Soc.* **2005**, *127* (27), 9670.

(37) Paramanathan, T.; Westerlund, F.; McCauley, M. J.; Rouzina, I.; Lincoln, P.; Williams, M. C. *J. Am. Chem. Soc.* **2008**, *130* (12), 3752.

(38) Bahira, M.; McCauley, M. J.; Almaqwashi, A. A.; Lincoln, P.; Westerlund, F.; Rouzina, I.; Williams, M. C. *Nucleic acids Res* **2015**, *43* (18), 8856.

(39) Ghosh, D.; Ahmad, H.; Thomas, J. *Chem. Commun.* **2009**, No. 20, 2947.

(40) Walker, M. G.; Jarman, P. J.; Gill, M. R.; Tian, X.; Ahmad, H.; Reddy, P. A. N.; McKenzie, L.; Weinstein, J. A.; Meijer, A. J. H. M.; Battaglia, G.; Smythe, C. G. W.; Thomas, J. A. *Chem. Eur. J.* **2016**, *22* (17), 5996.

(41) Metcalfe, C.; Webb, M.; Thomas, J. A. *Chem. Commun.* **2002**, No. 18, 2026.

(42) Metcalfe, C.; Haq, I.; Thomas, J. A. *Inorg Chem* **2004**, *43* (1), 317.

(43) Foxon, S. P.; Metcalfe, C.; Adams, H.; Webb, M.; Thomas, J. A. *Inorg Chem* **2007**, *46* (2), 409.

(44) Saeed, H. K.; Saeed, I. Q.; Buurma, N. J.; Thomas, J. A. *Chem. Eur. J.* **2017**, *23* (23), 5467.

(45) Jarman, P. J.; Saeed, I. Q.; McKenzie, L. K.; Weinstein, J. A.; Buurma, N. J.; Smythe, C. G. W.; Thomas, J. *Angew. Chem. Int. Ed.* **2017**, *56* (41), 12628.

(46) Foxon, S. P.; Phillips, T.; Gill, M. R.; Towrie, M.; Parker, A. W.; Webb, M.; Thomas, J. A. *Angew. Chem. Int. Ed.* **2007**, *46* (20), 3686.

(47) Sreedharan, S.; Gill, M. R.; Garcia, E.; Saeed, H. K.; Robinson, D.; Byrne, A.; Cadby, A.; Keyes, T. E.; Smythe, C.; Pellett, P.; Bernardino de la Serna, J.; Thomas, J. A. *J. Am. Chem. Soc.* **2017**, *139* (44), 15907.

(48) Bunville, L. G.; Geiduschek, E. P.; Rawitscher, M. A.; Sturtevant, J. M. *Biopolymers* **1965**, *3* (3), 213.

(49) Dore, E.; Frontali, C.; Gratton, E. *Biopolymers* **1972**, *11* (2), 443.

(50) Lando, D. Y.; Haroutiunian, S. G.; Kul ba, A. M.; Dalian, E. B.; Orioli, P.; Mangani, S.; Akhrem, A. A. *J. Biomol. Struct. Dyn.* **1994**, *12* (2), 355.

(51) McGhee, J. D. J.; Hippel, von, P. H. P. *J. Mol. Biol.* **1974**, *86* (2), 469.

(52) de Silva, A. P.; Gunaratne, H.; Gunnlaugsson, T.; Huxley, A.; McCoy, C. P.; Rademacher, J. T.; Rice, T. E. *Chem. Rev.* **1997**, *97* (5), 1515.

(53) Liu, Z.; He, W.; Guo, Z. *Chem Soc Rev* **2013**, *42* (4), 1568.

(54) la Cadena, De, A.; Davydova, D.; Tolstik, T.; Reichardt, C.; Shukla, S.; Akimov, D.; Heintzmann, R.; Popp, J.; Dietzek, B. *Sci. Rep.* **2016**, *6*, 33547.

(55) Fees, J.; Kaim, W.; Moscherosch, M.; Matheis, W.; Klima, J.; Krejcik, M.; Zalis, S. *Inorg Chem* **1993**, *32* (2), 166.

(56) Dyer, J.; Blau, W. J.; Coates, C. G.; Creely, C. M.; Gavey, J. D.; George, M. W.; Grills, D. C.; Hudson, S.; Kelly, J. M.; Matousek, P.; McGarvey, J. J.; McMaster, J.; Parker, A. W.; Towrie, M.; Weinstein, J. A. *Photochem. Photobiol. Sci.* **2003**, *2* (5), 542.

(57) Olson, E.; Hu, D.; Hörmann, A.; Jonkman, A. M.; Arkin, M. R.; Stemp, E.; Barton, J. K.; Barbara, P. F. *J. Am. Chem. Soc.* **1997**, *119* (47), 11458.

(58) Frisch, M. J.; Trucks, G. W.; Schlegel, H. B.; Scuseria, G. E.; Robb, M. A.; Cheeseman, J. R.; Scalmani, G.; Barone, V.; Mennucci, B.; Petersson, G. A.; Nakatsuji, H.; Caricato, M.; Li, X.; Hratchian, H. P.; Izmaylov, A. F.; Bloino, J.; Zheng, G.; Sonnenberg, J. L.; Hada, M.; Ehara, M.; Toyota, K.; Fukuda, R.; Hasegawa, J.; Ishida, M.; Nakajima, T.; Honda, Y.; Kitao, O.; Nakai, H.; Vreven, T.; Montgomery, J. A., Jr; Peralta, J. E.; Ogliaro, F.; Bearpark, M. J.; Heyd, J.; Brothers, E. N.; Kudin, K. N.; Staroverov, V. N.; Kobayashi, R.; Normand, J.; Raghavachari, K.; Rendell, A. P.; Burant, J. C.; Iyengar, S. S.; Tomasi, J.; Cossi, M.; Rega, N.; Millam, N. J.; Klene, M.; Knox, J. E.; Cross, J. B.; Bakken, V.; Adamo, C.; Jaramillo, J.; Gomperts, R.; Stratmann, R. E.; Yazyev, O.; Austin, A. J.; Cammi, R.; Pomelli, C.; Ochterski, J. W.; Martin, R. L.; Morokuma, K.; Zakrzewski, V. G.; Voth, G. A.; Salvador, P.; Dannenberg, J. J.; Dapprich, S.; Daniels, A. D.; Farkas, Ö.; Foresman, J. B.; Ortiz, J. V.; Cioslowski, J.; Fox, D. J. *Gaussian , Revision D.* **2009**.

(59) Becke, A. D. *J Chem Phys* **1993**, *98* (7), 5648.

(60) Grimme, S.; Ehrlich, S.; Goerigk, L. *J. Comput. Chem.* **2011**, *32* (7), 1456.

(61) Plasser, F. *TheoDORE ..*

(62) Hell, S. W. *Science* **2007**, *316* (5828), 1153.

(63) Clausen, M. P.; Galiani, S.; Bernardino de la Serna, J.; Fritzsche, M.; Chojnacki, J.; Gehmlich, K.; Lagerholm, B. C.; Eggeling, C. **2014**, *1* (1), 1.

(64) Blom, H.; Widengren, J. *Chem. Rev.* **2017**, *117* (11), 7377.

(65) Sednev, M. V.; Belov, V. N.; Hell, S. W. *Methods Appl Fluoresc* **2017**, *3* (4), 1.

(66) Fujiwara, Y.; Kikuchi, H.; Aizawa, S.; Furuta, A.; Hatanaka, Y.; Konya, C.; Uchida, K.; Wada, K.; Kabuta, T. *Autophagy* **2014**, *9* (8), 1167.

(67) Fujiwara, Y.; Wada, K.; Kabuta, T. *J Biochem* **2016**, *17*, mvw085.

(68) Chambron, J. C.; Sauvage, J.-P. *Chem. Phys. Lett.* **1991**, *182* (6), 603.

(69) Cook, N. P.; Torres, V.; Jain, D.; Martí, A. A. *J. Am. Chem. Soc.* **2011**, *133* (29), 11121.

(70) Cook, N. P.; Kilpatrick, K.; Segatori, L.; Martí, A. A. *J. Am. Chem. Soc.* **2012**, *134* (51), 20776.

(71) Cook, N. P.; Ozbil, M.; Katsampes, C.; Prabhakar, R.; Martí, A. A. *J. Am. Chem. Soc.* **2013**, *135* (29), 10810.

(72) Gill, M. R.; Cecchin, D.; Walker, M. G.; Mulla, R. S.; Battaglia, G.; Smythe, C.; Thomas, J. A. *Chem. Sci.* **2013**, *4* (12), 4512.

(73) Siddik, Z. H. *Oncogene* **2003**, *22* (47), 7265.

(74) Shen, D. W.; Pouliot, L. M.; Hall, M. D.; Gottesman, M. M. **2012**, *64* (3), 706.

(75) Zisowsky, J.; Koegel, S.; Leyers, S.; Devarakonda, K.; Kassack, M. U.; Osmak, M.; Jaehde, U. *Biochem. Pharmacol.* **2007**, *73* (2), 298.

(76) OpenEye toolkits 2018.Feb.1, OpenEye Scientific software, Santa Fe, NM. http://www.eyesopen.com